Generation of linear and nonlinear nonparaxial accelerating beams

Peng Zhang,[1,2] Yi Hu,[3] Drake Cannan,[2] Alessandro Salandrino,[1] Tongcang Li,[1] Roberto Morandotti,[3] Xiang Zhang,[1,4,6] and Zhigang Chen[2,5,*]

[1]*NSF Nanoscale Science and Engineering Center, 3112 Etcheverry Hall, University of California, Berkeley, California 94720, USA*

[2]*Department of Physics and Astronomy, San Francisco State University, San Francisco, California 94132, USA*

[3]*Institut National de la Recherche Scientifique, Varennes, Québec J3X 1S2, Canada*

[4]*Materials Science Division, Lawrence Berkeley National Laboratory, 1 Cyclotron Road, Berkeley, California 94720, USA*

[5]*TEDA Applied Physics School, Nankai University, Tianjin 300457, China*

[6]*e-mail: xiang@berkeley.edu*

**Corresponding author: biglasers@gmail.com*

Received April 10, 2012; accepted May 2, 2012;
posted May 7, 2012 (Doc. ID 166290); published July 9, 2012

We study linear and nonlinear self-accelerating beams propagating along circular trajectories beyond the paraxial approximation. Such nonparaxial accelerating beams are exact solutions of the Helmholtz equation, preserving their shapes during propagation even under nonlinearity. We generate experimentally and observe directly these large-angle bending beams in colloidal suspensions of polystyrene nanoparticles. © 2012 Optical Society of America

OCIS codes: 070.7345, 190.4420, 190.3970.

Recently, self-accelerating Airy beams [1,2] have attracted a great deal of interest. In contraposition with Bessel beams [3], Airy beams are solutions of the paraxial wave equation which do not rely on simple conical superposition of plane waves. For the past five years, research efforts on Airy beams have spanned from fundamental aspects to demonstration of possible applications [4]. In practice, all nondiffracting Airy beams must be truncated to keep the energy finite and such truncated beams eventually diffract and lose their unique structures after long propagation. One possibility is to use nonlinearity for self-trapping of Airy beams, leading to a soliton-like propagation of self-accelerating beams [5–7]. Limited by their paraxial nature, Airy beams cannot maintain their shape-preserving property when bending to larger angles. Thus, it is important to identify mechanisms that could allow accelerating beams to propagate in a true diffraction-free manner even during large trajectory bending [8–10]. In a recent study, self-accelerating beams have been extended to the nonparaxial regime, where one could expect such beams to travel, in principle, along circular trajectories with preserving shapes [11].

In this letter, we present experimental demonstration of linear and nonlinear nonparaxial accelerating beams (NABs) propagating along a circular trajectory. Theoretically, with the approach developed by Kaminer *et al.* [11,12], we show that these NABs as found from the Helmholtz equation without the paraxial approximation preserve their shapes even under different nonlinearities. Experimentally, we generate these NABs with a spatial light modulator (SLM) and observe their large-angle bending paths in colloidal suspension of polystyrene nanoparticles. We discuss the differences between the NABs and paraxial Airy beams, as well as between the linear and nonlinear NABs.

Let us start from the scalar Helmholtz equation [5,6]

$$\frac{\partial^2 U}{\partial x^2}+\frac{\partial^2 U}{\partial z^2}+k_0^2(n_0+\Delta n)^2U=0, \tag{1}$$

where $U(x,z)$ is the complex amplitude of the light field propagating along z, $k_0=2\pi/\lambda$ is the wave number in vacuum and n_0 is the refractive index of the medium. The nonlinear term $\Delta n=\gamma|U|^2$ (γ is the nonlinear coefficient) determines the light-induced refractive index change under the Kerr effect. According to the symmetry of the equation, we seek the accelerating shape-preserving beams in a polar coordinate system with $U(r)=u(r)\exp(i\beta\theta)$, where $r=z/\sin\theta=x/\cos\theta$ and β is a real constant. For $\Delta n\ll n_0$, Eq. (1) becomes

$$\frac{d^2u}{dr^2}+\frac{1}{r}\frac{du}{dr}-\frac{\beta^2}{r^2}u+k_0^2n_0^2u+2k_0^2n_0\gamma u^3=0. \tag{2}$$

By directly solving Eq. (2) at $\gamma=0$ and $\gamma\neq 0$, solutions for both linear and nonlinear accelerating beams can be obtained without using the paraxial approximation.

By setting $\gamma=0$, Eq. (2) turns into a Bessel's differential equation with a typical solution of $u(r)=J_\beta(kr)$, where $k=n_0k_0$. Therefore, the linear NAB in Cartesian coordinate system reads as

$$U(x,z)=J_\beta\left(k\sqrt{x^2+z^2}\right)\exp(i\beta\times\arctan(z/x)). \tag{3}$$

Apparently, such a NAB accelerates along a closed circular trajectory but requires infinite energy and both forward and backward propagating components to form a longitudinal vortex of order β in the x-z plane. To physically realize the NAB, we introduce a truncated NAB with an exponential aperture and a Heaviside step function $H(x)$, which has the following form at $z=0$

$$U(x,0)=\exp(-\alpha x)H(x+\beta/k)J_\beta(kx+\beta). \tag{4}$$

Note that the main lobe of the truncated NAB is shifted close to zero and it only contains the forward propagating component, resulting in a maximum self-bending of 180° along a half-circle. The Fourier spectrum associated with such a NAB without exponential truncation reads as

$$\psi(f_x) = (k^2 - f_x^2)^{-1/2} \exp(i\beta(f_x/k - \arcsin(f_x/k))), \quad (5)$$

where f_x represents the transverse spatial frequency. From Eq. (5), one can readily deduce the phase structure for the generation of the NAB using a Fourier transformation method, similar to the case for Airy beams [4].

To highlight the difference between NABs and paraxial Airy beams, some detailed comparisons are juxtaposed in Fig. 1, where (a) and (c) depict the beam profiles and the phase profile of their angular Fourier spectra of a linear NAB (solid, blue) and of an Airy beam (dashed, red) with a same main-lobe width at $z = 0$.

Although the NAB and Airy beam look very similar both in the real space and in the k-space, one can notice the relatively larger spacing between humps in the "tail" and a steeper phase change in the boundary of the spectrum for the NAB. We shall show that, due to these subtle differences, the propagation behaviors of the two beams are dramatically different. Figure 1(b) depicts the intensity profiles of the NAB and Airy beam after linearly propagating to $z = R/2$ ($R \approx \beta/k$ is the radius of the circular path of the NAB, here $\beta = 150$, $\lambda = 532$ nm, and $n_0 = 1.33$). The side-view propagations of the two beams are displayed in Figs. 1(d) and 1(e), where the beams are launched at $z = -3R/2$ and propagate to the right under nonparaxial conditions. Clearly, the NAB bends to a much larger angle and meanwhile preserves the beam shape to a much longer propagation distance as compared to the paraxial Airy beam.

In presence of the Kerr nonlinearity, the nonlinear NABs can be obtained by numerically solving Eq. (2). A typical nonlinear solution at $\gamma = 0.1$ and its nonlinear propagation are shown in Figs. 2(a) and 2(b). Clearly, such a nonlinear NAB maintains its beam shape during propagation along a circular path in spite of the nonlinearity. In practice, the nonlinear NABs can be excited by propagating the linear NABs under the action of nonlinearity. Figures 2(c)–2(e) depict the nonlinear evolution of the linear NAB shown in Fig. 1(e). Indeed, instead of being broken up by the nonlinearity [5], the linear NAB evolves into a nonlinear NAB, preserving the accelerating property. Figures 2(c) and 2(d) directly compare the intensity profiles of the linear and nonlinear NABs at $z = 0$ and $R/2$ [marked by two dashed lines in Fig. 2(e)]. When compared

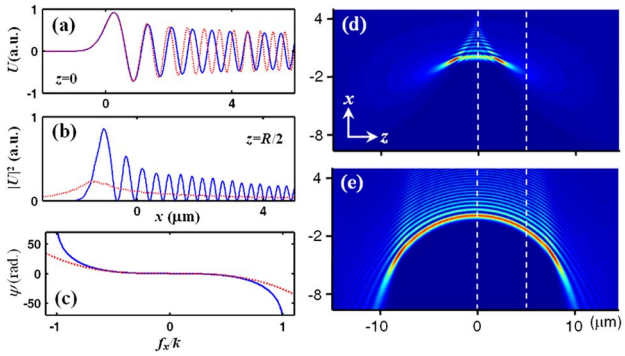

Fig. 1. (Color online) (a) Amplitude of a linear NAB (solid, blue) and an Airy beam (dashed, red) with the same main lobe size; (b) intensity profiles of the NAB and Airy beam in (a) after linear propagation of $z = R/2$; (c) phase profile of Fourier spectra of the NAB and the Airy beam in (a); (d), (e) Sideview propagation of the Airy beam (d) and the NAB (e) in (a).

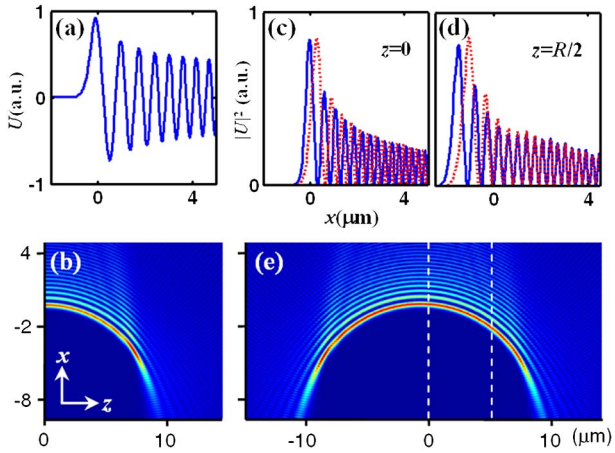

Fig. 2. (Color online) Numerical solution (a) and its propagation (b) for a *nonlinear* NAB; (c)–(e) depicts nonlinear evolution of the NAB with initial condition shown in Fig. 1(a), where (c) and (d) are intensity profiles after linear (dashed) and nonlinear (solid) propagation to $z = 0$ and $R/2$, as marked by the dashed lines in the side view (e).

to the linear propagation, the main lobe of the nonlinear NAB is slightly narrower and has a noticeable lateral shift under nonlinear propagation. Our simulation using the saturable nonlinearity found qualitatively similar results.

To generate the linear and nonlinear accelerating beams illustrated in Figs. 1 and 2, we use the experimental setup sketched in Fig. 3. Instead of directly Fourier transforming the phase mask determined by Eq. (5) as in our prior work on Airy beams [5,13], here we employ the computer generated holography, which has proved to be an effective way for demonstrating auto-focusing beams and optical bottle beams [14,15]. Specifically, a Gaussian beam ($\lambda = 532$ nm) is sent through a SLM programmed with an off-axis hologram of the desired phase profile. Such a hologram is produced by computing the interference between the phase profile of the Fourier spectrum of an accelerating beam and a plane wave, as shown in the inset of Fig. 3. Upon reflection from the hologram in the SLM, the encoded phase information is reconstructed via a spatial filtering $4f$-system. Then it is Fourier transformed through an objective lens to generate the designed NAB, passing through a glass cuvette containing 100 nm polystyrene beads suspended in water at 0.1 wt.% concentration. The top-view of the beam is captured by a high-resolution camera, and the transverse beam patterns at different propagation distances are monitored by a CCD.

To directly compare the *linear* propagation property of a NAB with that of an Airy beam, a Nikon 60× water immersion objective with a numerical aperture (NA) of

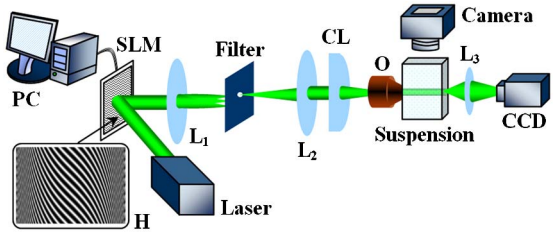

Fig. 3. (Color online) Experimental setup for the generation of NABs. SLM, spatial light modulator; H, computer generated hologram; L, lens; CL, cylindrical lens; O, microscope objective.

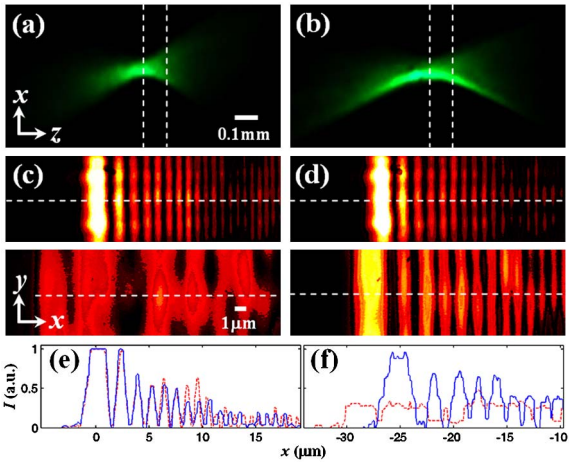

Fig. 4. (Color online) Experimental side-view photography of the *linear* propagation of (a) an Airy beam and (b) a NAB taken from scattered light; (c), (d) transverse patterns taken at $z = 0$ and $z = 0.1$ mm positions as marked by dashed lines in (a), (b) where (c) and (d) correspond to the Airy beam and the NAB, and top and bottom panels correspond to $z = 0$ ($z = 0.1$ mm) propagation distance; (e), (f) Intensity profiles taken along the dashed line marked in (c), (d) from the Airy beam (dashed) and the NAB (solid). (e) is taken from $z = 0$ and (f) from $z = 0.1$ mm.

1.0 is used. The experimental results are shown in Fig. 4, where (a) and (b) provide a direct top-view of the scattered light from the generated paraxial Airy beam and the NAB, respectively. Clearly, the Airy beam cannot keep its shape after about 0.1 mm of propagation distance, while the NAB preserves its shape after a large-angle bending. Snapshots of transverse intensity patterns of the two beams are displayed in Figs. 4(c)–4(d), taken at $z = 0$ and $z = 0.1$ mm as marked by the dashed lines in (a) and (b). Together with the intensity profiles shown in (e) and (f), it can be clearly seen that the NAB preserves its structure much better than the Airy beam does, in agreement with results from numerical simulations.

To demonstrate *nonlinear* propagation of the nonparaxial beam, we use the artificial Kerr nonlinearity offered by nanosuspensions [16]. Considering the beam and particle sizes, we use a 20× objective lens with 0.4 NA to create the accelerating beam. By increasing the laser power from 10 μW to about 30 mW, linear and nonlinear propagation of the NAB can be directly observed as shown in Fig. 5, where (a) and (b) are the direct top-view photography. The transverse intensity patterns [Fig. 5(c)] are taken by the CCD camera through imaging the beam exiting the 1 mm long cuvette. Our experimental results clearly demonstrate that the NAB maintains its shape-preserving property even under nonlinear propagation. Although the difference between linear and nonlinear propagation is quite subtle at the output plane, a lateral shift and self-narrowing of the main lobe of the NAB under nonlinear propagation are evident, as expected from our numerical simulations.

In summary, we have reported the experimental observation of NABs and their propagation through colloidal nanosuspensions. Such nondiffracting and large-angle self-bending beams may find applications in particle manipulation [15] and surface plasmon routing [17–19].

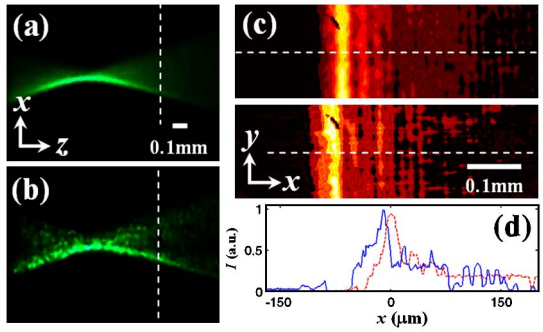

Fig. 5. (Color online) Experimental side-view photography of (a) linear and (b) nonlinear NAB. (c) Transverse output patterns taken at about $z = 1$ mm as marked by dashed line in (a), (b), where top and bottom panels correspond to patterns from (a) and (b), respectively. (d) Linear (dashed) and nonlinear (solid) output intensity profiles taken along dashed line in (c).

This work was supported by the US ARO MURI program (W911NF-09-1-0539), AFOSR, and the NSF Nano-scale Science and Engineering Center (CMMI-0751621) and PHY-1100842. Y. H. acknowledges support from MELS FQRNT Fellowship. We thank M. Segev for discussion.

References

1. G. A. Siviloglou and D. N. Christodoulides, Opt. Lett. **32**, 979 (2007).
2. G. A. Siviloglou, J. Broky, A. Dogariu, and D. N. Christodoulides, Phys. Rev. Lett. **99**, 213901 (2007).
3. J. Durnin, J. J. Miceli, Jr., and J. H. Eberly, Phys. Rev. Lett. **58**, 1499 (1987).
4. Y. Hu, G. A. Siviloglou, P. Zhang, N. K. Efremidis, D. N. Christodoulides, and Z. Chen, in *Nonlinear Photonics and Novel Phenomena*, Z. Chen and R. Morandotti, eds. (Springer, 2012).
5. Y. Hu, S. Huang, P. Zhang, C. Lou, J. Xu, and Z. Chen, Opt. Lett. **35**, 3952 (2010).
6. I. Kaminer, M. Segev, and D. N. Christodoulides, Phys. Rev. Lett. **106**, 213903 (2011).
7. A. Lotti, D. Faccio, A. Couairon, D. G. Papazoglou, P. Panagiotopoulos, D. Abdollahpour, and S. Tzortzakis, Phys. Rev. A **84**, 021807 (2011).
8. A. V. Novitsky and D. V. Novitsky, Opt. Lett. **34**, 3430 (2009).
9. A. Torre, Opt. Commun. **283**, 4146 (2010).
10. L. Froehl, L. Froehly, F. Courvoisier, A. Mathis, M. Jacquot, L. Furfaro, R. Giust, P. A. Lacourt, and J. M. Dudley, Opt. Express **19**, 16455 (2011).
11. I. Kaminer, R. Bekenstein, J. Nemirovsky, and M. Segev, Phys. Rev. Lett. **108**, 163901 (2012).
12. I. Kaminer and M. Segev, "Sub-wavelength nonlinear accelerating beams," submitted to *OSA Topical Meeting*, *Nonlinear Photonics* (2012).
13. Y. Hu, P. Zhang, C. Lou, S. Huang, J. Xu, and Z. Chen, Opt. Lett. **35**, 2260 (2010).
14. P. Zhang, Z. Zhang, J. Prakash, S. Huang, D. Hernandez, M. Salazar, D. N. Christodoulides, and Z. Chen, Opt. Lett. **36**, 1491 (2011).
15. P. Zhang, J. Prakash, Z. Zhang, M. S. Mills, N. K. Efremidis, D. N. Christodoulides, and Z. Chen, Opt. Lett. **36**, 2883 (2011).
16. A. Ashkin, J. M. Dziedzic, and P. W. Smith, Opt. Lett. **7**, 276 (1982).
17. P. Zhang, S. Wang, Y. Liu, X. Yin, C. Lu, Z. Chen, and X. Zhang, Opt. Lett. **36**, 3191 (2011).
18. A. Minovich, A. E. Klein, N. Janunts, T. Pertsch, D. N. Neshev, and Y. S. Kivshar, Phys. Rev. Lett. **107**, 116802 (2011).
19. L. Li, T. Li, S. M. Wang, C. Zhang, and S. N. Zhu, Phys. Rev. Lett. **107**, 126804 (2011).